OXFORD UNIVERSITY PRESS | Human Molecular Genetics

Dominant and recessive mutations in rhodopsin activate different cell death pathways

Journal:	*Human Molecular Genetics*
Manuscript ID	HMG-2016-D-00174.R1
Manuscript Type:	2 General Article - UK Office
Date Submitted by the Author:	n/a
Complete List of Authors:	Comitato, Antonella; University of Modena, Department of Life Sciences Di Salvo, Maria Teresa; University of Modena, Department of Life Sciences Turchiano, Giandomenico; University of Modena, Department of Life Sciences Montanari, Monica; University of Modena, Department of Life Sciences Sakami, Sanae; Case Western University, Pharmacology Palczewski, Krzysztof; Case Western University, Pharmacology; Marigo, Valeria; University of Modena, Department of Life Sciences
Key Words:	retinitis pigmentosa, apoptosis, neuroprotection, rhodopsin

Dominant and recessive mutations in rhodopsin activate different cell death pathways

Antonella Comitato[1], Maria Teresa Di Salvo[1], Giandomenico Turchiano[1,§], Monica Montanari[1], Sanae Sakami[2], Krzysztof Palczewski[2], Valeria Marigo[1,*]

[1]Department of Life Sciences, University of Modena and Reggio Emilia, 41125 Modena, Italy

[2]Department of Pharmacology, Cleveland Center for Membrane and Structural Biology, School of Medicine, Case Western Reserve University, Cleveland, OH 44106, USA

[§]Current address: Institute for Cell and Gene Therapy & Center for Chronic Immunodeficiency - University of Freiburg, Freiburg, Germany

[*]Corresponding Author: Valeria Marigo, Department of Life Sciences, University of Modena and Reggio Emilia, via Campi, 287, 41125 Modena, Italy; phone: +390592055392; fax: +390592055410; email: valeria.marigo@unimore.it

Abstract

Mutations in rhodopsin (RHO) are a common cause of retinal dystrophy and can be transmitted by dominant or recessive inheritance. Clinical symptoms caused by dominant and recessive mutations in patients and animal models are very similar but the molecular mechanisms leading to retinal degeneration may differ. We characterized three murine models of retina degeneration caused by either Rho loss of function or expression of the P23H dominant mutation in Rho. Rho loss of function is characterized by activation of calpains and apoptosis-inducing factor (Aif) in dying photoreceptors. Retinas bearing the P23H dominant mutations activate both the calpain-Aif cell death pathway and ER-stress responses that together contribute to photoreceptor cell demise. *In vivo* treatment with the calpastatin peptide, a calpain inhibitor, was strongly neuroprotective in mice lacking Rho while photoreceptor survival in retinas expressing the P23H dominant mutation was more affected by treatment with salubrinal, an inhibitor of the ER-stress pathway. The further reduction of photoreceptor cell demise by co-treatment with calpastatin and salubrinal suggests co-activation of the calpain and ER-stress death pathways in mice bearing dominant mutations in the *Rho* gene.

Introduction

Retinitis pigmentosa (RP) is an inherited form of retinal degeneration characterized by progressive loss of the peripheral visual field leading to tunnel vision and finally blindness. Patients experience difficulties with dark adaptation and night blindness in adolescence followed by loss of the mid-peripheral visual field in young adulthood (1). Visual symptoms mirror the progressive loss of rod photoreceptors. Causative mutations for RP have been identified in several genes (Retnet database: http://www.sph.uth.tmc.edu/retnet). These genes encode proteins with very diverse functions and patterns of expression, which can be restricted to rods or be expressed by several neurons in the human retina (http://rpexp.tigem.it/; (2)). Mutations in *Rhodopsin* (*RHO*) represent a common cause of RP, accounting for 25% of autosomal dominant RP (adRP) and 8 to 10% of all RP (1) with more than 100 different associated mutations identified so far (http://www.hgmd.cf.ac.uk). Impairment of the phototransduction cascade caused by RHO loss of function is linked to autosomal recessive Retinitis Pigmentosa (arRP) and congenital night blindness (CNB) (3, 4). The molecular mechanisms underlying cell death caused by either dominant or recessive mutations in RHO are still not well characterized.

RHO is a G-protein coupled receptor localized to rod outer segments where the phototransduction cascade is initiated. RHO is the most abundant protein produced by rod cells accounting for 30% of their total protein content and is particularly enriched, up to 90%, in the rod outer segments (5–7). Data regarding the pathogenic mechanism(s) of mutant RHO are still controversial. Accumulation of mutant RHO in different subcellular compartments, including the endoplasmic reticulum (ER), may trigger the unfolded protein response (UPR) with cytoprotective outputs that reduce protein synthesis and up-regulate chaperones to cope with stress (8). Excessive mutant RHO accumulation can then lead to ER-stress responses that culminate with cell death (9). ER-stress and other mechanisms

involving the ER-associated degradation (ERAD) pathway and autophagy have been linked to RHO mutation and may all contribute to retinal degeneration (10, 11). Saliba and colleagues reported that exposure of p.Pro23His (P23H) mutant RHO, the most common mutation in USA (12), to 9-*cis*-retinal in transfected cells increased plasma membrane localization of the mutant protein but did not decrease the formation of aggresomes or their detrimental effects (13). Murine models to study effects caused by mutant RHO and specifically the P23H mutation are available as transgenic mice and rats (14, 15) that suffer a very severe form of retinal degeneration. More recently, two knock-in mouse models were generated for the P23H mutation and they show a much slower progression of the disease (16, 17).

Quality control during protein synthesis imposed by the ER activates ER resident sensors involved in the UPR to allow only properly folded proteins to leave the organelle. Expression of mutant proteins may affect cellular ability to cope with UPR causing the cell to activate ER-stress and succumb to apoptosis. The transducers of the UPR/ER-stress responses are ER resident proteins: the inositol-requiring enzyme 1 (Ire1), the activating transcription factor-6 (Atf6) and the protein kinase R-like ER protein kinase (Perk). Ire1 is a ribonuclease that, when activated, splices the mRNA encoding X-box transcription factor 1 (*Xbp1*), leading to a frame shift and production of sXbp1, a transcription factor regulating expression of chaperones. The Perk pathway is characterized by phosphorylation of Perk and eukaryotic initiation factor-2α (eIF2α) resulting in reduction of protein synthesis and up-regulation of Atf4 that regulates expression of several cell death related genes (18).

We previously showed that calpain activation as well as nuclear translocation of Aif (Apoptosis-inducing factor) play fundamental roles in photoreceptor cell death in the retinal degeneration 1 (*rd1*) mouse model (19, 20). Aif is a mitochondrial protein that can be cleaved by calpains, leaves the mitochondrion through a pore formed by Bax and recruits

Cyclophilin A for chromatin fragmentation (21, 22). Aif, as well as ER-stress, were reported to be activated in P23H transgenic rodents (23–25).

In this study we characterized the interrelationship of these calpain-mediated and ER stress-mediated cell death pathways in Rhodopsin mutant mice. Specifically, we compared the Rho knock-out mouse, a model for arRP, with two lines of mice expressing P23H mutant Rho, models for adRP. We isolated expression of the P23H mutation from wild type Rho in one of the two models to uncover molecular cytotoxic mechanisms activated by the dominant mutation. Co-expression of wild type Rho, in fact, alleviates the phenotype and may hinder the characterization of molecular pathways (9). We characterized the different contributions of the two pathways by *in vivo* treatments with drugs targeting either calpains or ER-stress. We demonstrated that Rho loss of function did not activate ER-stress pathways but induced cell death through activation of calpains. In photoreceptors bearing the P23H dominant mutation both pathways were activated but ER stress appeared to play a critical role. Finally, we showed the protective effects in more than one murine model by targeting both pathways with a drug combination.

Results

Activation of Calpains and Aif in dying rod cells bearing mutations in the *Rho* gene

To study the molecular effects of a dominant compared to a recessive mutation in the *Rho* gene, we evaluated cell death pathways activated in rod photoreceptors. We analyzed the transgenic mouse expressing human P23H RHO ($P23H^{Tg}$) (14), the knock-in P23H mouse (17) bred to eliminate the wild type Rho allele ($Rho^{P23H/-}$) and compared them to the homozygous Rho knock-out mouse ($Rho^{-/-}$) (26). We chose to study the P23H mutation in the absence of wild type Rho in one of the murine models to uncover molecular mechanisms activated by the mutation and limit protecting effects from the wild type protein (9). The peaks of cell death in the retinas of these chosen murine models were post-natal day 9 (PN9) for $P23H^{Tg}$, PN16 for $Rho^{P23H/-}$ and PN45 for $Rho^{-/-}$ (as reported in (27) and shown in Figure S1 A). Lack of the wild type allele in the $Rho^{P23H/-}$ retina caused a more rapid degeneration compared to the published phenotype in $Rho^{P23H/+}$ (17, 28). Previous studies reported that the P23H mutation did not cause a reduction of *Rho* mutant mRNA rather lower levels of P23H mutant Rho protein as well as unpaired glycosylation (16, 17). We thus analyzed Rho protein in mutant retinas from $Rho^{P23H/-}$ and $P23H^{Tg}$ (in the absence of the endogenous wild type allele) before and at their peaks of cell death. Here the P23H mutant Rho monomer (open arrow) appeared less abundant compared to wild type Rho at the same age (Figure S1 B), in line with reports analyzing expression of Rho in $Rho^{P23H/P23H}$ retinas and other mutant alleles expressed in the absence of wild type Rho (9, 17, 28). Retinas expressing only P23H mutant Rho had more forms at higher molecular weights that probably represent aggregates/multimers, as reported *in vitro* and *in vivo* for dominant RHO mutations (9, 29–31). Moreover, immunofluorescence analyses showed accumulation of P23H mutant Rho around the nuclei of photoreceptors suggesting that it aggregates inside the cells (Figure S1 C).

We previously characterized the molecular pathways of cell death in the *rd1* mouse model of RP and showed that calpain and Aif play key roles in photoreceptor demise (19, 27). Activation of calpains was reported in several rodent models of RP and we reported calpain activation in *P23H*^{Tg} and *Rho*$^{-/-}$ degenerating retinas (32, 33). In this study we confirmed activation of calpains in all the chosen mouse models by assessing the cleavage of αII-spectrin, a substrate for calpains (34) as well as by using the previously published *in situ* calpain activity assay (19, 20, 27). Protein analysis confirmed an increase of the 145 kDa fragment of αII-spectrin consistent with cleavage by calpains (Figure 1 A, arrow). Retinas expressing P23H mutant Rho also showed 120 kDa fragments possibly derived from activation of caspases (asterisk). Here we *in situ* confirmed activation of calpains also in *Rho*$^{P23H/-}$ photoreceptors at PN16 (Figure S1 D). Double labeling of calpain activity with TUNEL indicated that about 50% of dying cells in PN9 *P23H*^{Tg} and PN16 *Rho*$^{P23H/-}$ retinas activated calpains while calpains contributed more prominently to cell death in the *Rho*$^{-/-}$ mutant retina by labeling about 90% of TUNEL^{+} cells (Figure 1 B).

We then evaluated Aif activation and nuclear translocation by immunofluorescence imaging and immunoblotting of nuclear extracts derived from wild type and Rho mutant retinas. Aif translocation into the photoreceptor nuclei of these three murine models was high at their peaks of cell death (Figure 1 C, arrows and Figure S1 E-G). We counted cells with nuclear localization of Aif that were co-labeled by TUNEL and found that about 50% of both *P23H*^{Tg} and *Rho*$^{P23H/-}$ dying cells showed Aif inside their nuclei, similar to cells activating calpains (Figure 1 D). A stronger correlation of Aif activation with TUNEL was observed in *Rho*$^{-/-}$ retinas (Figure 1 D). Aif translocation into the nuclei of dying photoreceptor cells was confirmed by immunoblotting that compared nuclear extracts from wild type and mutant retinas (Figure1 E). Altogether these data demonstrate that calpains

are activated and Aif translocates into the nuclei of photoreceptor cells in mouse models of RP caused by Rho mutations.

Activation of calpains can be induced by increase of intracellular calcium as reported in the *rd1* mutant retina (19, 34). Using a fluorescent dye we compared calcium levels in wild type and mutant photoreceptors and found more photoreceptor cells with high levels of calcium in retinas bearing mutations in Rho (Figure S2).

Calpains activate Aif in Rho mutant retinas

To address whether Aif is activated by calpains in Rho mutant retinas we injected mice intravitreally with the calpain-specific inhibitor calpastatin peptide either at PN9 ($P23H^{Tg}$) or at PN15 ($Rho^{P23H/-}$) or at PN44 ($Rho^{-/-}$). Retinas were analyzed at PN10 for $P23H^{Tg}$, PN16 for $Rho^{P23H/-}$ and PN45 for $Rho^{-/-}$, respectively. The injection protocol was similar to the previously published method (20). Effectiveness of calpastatin peptide treatment was confirmed by the reduction of the 145 kDa fragment of αII-spectrin (Figure 2 A, arrow). We also observed a significant reduction of the number of photoreceptors activating calpains, based on the *in situ* calpain activity assay (Figure 2 B). Sixteen hours after calpastatin peptide injection, we detected a strong reduction of cell death in $Rho^{-/-}$ retinas as defined by the loss of TUNEL labeled cells as well as a decrease of cells showing activation of Aif (Figure 2 C-E). Activated Aif protein inside the nuclei was undetectable in $Rho^{-/-}$ retinas after treatment with calpastatin peptide (Figure 2 C). Calpain inhibition was thus very effective in reducing cell demise in retinas bearing recessive mutations in the *Rho* gene. Calpastatin peptide, significantly but at a lower level, reduced cell death and Aif nuclear translocation in retinas expressing the P23H mutation (Figure 2 C-E). This limited effect of calpain inhibition implies that calpains and Aif are not the only cell death factors triggered in photoreceptors cells expressing dominant mutations in Rho.

Activation of ER-stress in P23H Rho mutant rods

Activation of ER-stress was previously shown in rodent P23H mutant retinas (23, 35). We wished to define the timing of activation of Ire1 and Perk ER-stress sensors in our murine models expressing mutant Rho and correlate this to cell death as defined by TUNEL staining. No activation of ER stress sensors was detectable in *Rho*$^{-/-}$ retinas at any time point during degeneration (data not shown), thus the homozygous recessive model was not further analyzed in this study. Activation of Ire1, defined by detection of phosphorylated Ire1, was observed in *P23H*^{Tg} retinas with a marked decrease at PN10 (Figure 3 A). To confirm that Ire1 phosphorylation activated the pathway, we evaluated the alternative splicing of *Xbp1* with specific primers for spliced *Xbp1* (s*Xbp1*). Splicing of *Xbp1* (*sXbp1*) detectable at PN8 and PN9 but not at PN10 confirmed that activation of the Ire1 pathway declined with progression of retinal degeneration (Figure 3 B). Using antibodies for phosphorylated Ire1 we confirmed that phosphorylation of the ER-stress sensor Ire1 resided in photoreceptor cells and not in other retinal cells (Figure 3 C, arrow). Similar results were obtained by analyzing Ire1 phosphorylation and *Xbp1* splicing in *Rho*$^{P23H/-}$ retinas (Figure 4 A-C). The Perk pathway otherwise was activated at all evaluated time points during retinal degeneration in both mutant retinas as demonstrated by phosphorylation of Perk as well as by phosphorylation of Eif2α (Figure 3 D-E and Figure 4 D-E). We also confirmed that activation of the Perk pathway occurred in photoreceptor cells by immunofluorescence of retinal sections with the anti-phospho-Perk antibody (Figure 3 F and Figure 4 F).

Rods bearing a dominant mutation in Rho not only activate the calpain-Aif pathway but also the detrimental ER-stress pathways that together may contribute to retinal

degeneration. The individual impact of each of these pathways was tested by *in vivo* treatments with specific inhibitors.

Calpains and ER-stress contributions to cell death in P23H mutant photoreceptors

To test the impact of calpains on ER-stress we treated *P23H*^{Tg} and *Rho*$^{P23H/-}$ degenerating eyes *in vivo* with the calpastatin peptide and evaluated activations of ER-stress sensors. *P23H*^{Tg} eyes were intravitreally injected at the age of PN9 with calpastatin peptide and analyzed 16 hours later; Rho$^{P23H/-}$ eyes were intravitreally injected at the age of PN15 with calpastatin peptide and analyzed 16 hours later. The calpain inhibition had no significant effect on Ire1 activation (Figure 5 A-D and Figure S3 A-D) nor on the Perk pathway (Figure 5 E-H and Figure S3 E-H). Blocking calpains, however, significantly reduced cell death in both murine models expressing the P23H mutation (Figure 2E and Figure 5M).

We then interfered *in vivo* with ER-stress by intraperitoneal injection of salubrinal, an inhibitor of Eif2α dephosphorylation and thus of ER-stress (36). Salubrinal protected *P23H*^{Tg} rod photoreceptors from cell death reducing by 74% the number of TUNEL positive cells and by 50% *Rho*$^{P23H/-}$ mutant photoreceptors (Figure 5 M). Immunoblottings confirmed that salubrinal increased Eif2α phosphorylation in the retina without increased activation of Perk (Figure 5 E-H and Figure S3 E-H). We observed that salubrinal maintained higher levels of phosphorylated Ire1 and spliced *Xbp1* in PN10 *P23H*^{Tg} retinas and in PN16 *Rho*$^{P23H/-}$ retinas (Figure 5 A-D and Figure S3 A-D), ages when phosphorylated Ire1 is reduced (see Figures 3 A-B and Figure 4 A-B). The protective effect of salubrinal may thus be mediated by a sustained UPR. Salubrinal treatment had no effect on calpains because it did not reduce the number of photoreceptor cells activating calpains in *P23H*^{Tg} and in *Rho*$^{P23H/-}$ retinas (Figure 5 N). After interference of ER-stress with salubrinal, nuclear translocation of Aif was significantly affected in *P23H*^{Tg} and in

Rho$^{P23H/-}$ as defined by nuclear translocation analyses (Figure 5 I-J and Figure S3 I-J) and by counting cells double labeled by nuclear Aif and TUNEL (Figure 5 O).

Bip/Grp79 is a member of the Hsp70 family of chaperones that regulate ER stress signaling by binding to Ire1 and Perk. Over-expression of Bip/Grp79 in P23H mutant retinas was previously reported to be protective and to reduce retinal degeneration (23). We thus analyzed the Bip/Grp79 in retinas before and after treatments and found that salubrinal, but not calpastatin, increased Bip/Grp79 protein levels (Figure 5 K-L and Figure S3 K-L).

Targeting Calpains and ER-stress has additive protective effects in rod photoreceptors expressing P23H mutant Rho

Data described so far could not define if the different treatments were blocking the same cell death pathway at different levels or were interfering with different pathways activated in parallel. To address this question we co-treated mice with salubrinal and calpastatin peptide *in vivo*. The effects of salubrinal on the ER stress sensors were maintained also in the presence of calpastatin peptide, as demonstrated by increase in phosphorylation of Eif2α and of Ire1 (Figure 5 A-H and Figure S3 A-H). The combined treatment with salubrinal and calpastatin peptide also increased the levels of Bip/Gpr79 protein in both murine models expressing the P23H mutant Rho (Figure 5 K-L and Figure S3 K-L). This treatment had a stronger protective effect than either drug alone. In fact, we could measure a significant reduction of TUNEL^{+} cells (Figure 5 M) when compared to treatments with calpastatin peptide in both *P23H*^{Tg} and *Rho*$^{P23H/-}$ retinas. Decrease of cell death with the combined treatment was significant when compared to treatment with salubrinal only in *P23H*^{Tg} but not in *Rho*$^{P23H/-}$ retinas. Histological analyses show no evidence of toxic effects on photoreceptors or other retinal neurons after treatments

(Figure S4 A, C, D). The short time frame between injections and analyses helps biochemical studies but does not allow assessment of phenotype rescue with an increased number of photoreceptor cells or redistribution of the RHO protein (Figure S4).

Discussion

In this study we report a molecular characterization of cell death pathways in one model of recessive RP caused by Rho loss of function and two models of dominant RP caused by point mutations in Rho. The most interesting finding is a common mechanism of cell death, the calpain-mediated pathway, associated with both recessive and dominant Rho mutations. Interestingly, activation of calpains appears to be a general mechanism initiated by photoreceptors during retinal degeneration since calpains have been found activated in several animal models of RP (19, 20, 24, 25, 27, 33, 34, 37–41). The key role of calpains in retinal degeneration was also demonstrated after light damage on a canine model of RP bearing a mutation in the *RHO* gene (42). We also show co-activation of calpains and Aif suggesting that calpains may activate Aif in response to mutations of Rho similar to what we previously reported in the *rd1* mutant retinas (19). The reduction of Aif activation in retinas treated with calpastatin peptide, a calpain inhibitor, confirms this hypothesis. Calpastatin peptide is able to completely abolish Aif nuclear translocation as well as cell death in the $Rho^{-/-}$ retina but not in retinas expressing the P23H dominant mutation. This indicates that the main cell death pathway activated in RP linked to recessive mutation in *Rho* is mediated by calpains. We cannot exclude involvement of other mechanisms of cell death but prolonged exposure to calpain inhibitors will be required to uncover other players.

Activation of Aif appears to be mediated by calpains in all mutant retinas studied here, however expression of the dominant mutation may trigger other mechanisms that affect

activation of Aif. In fact, in both animal models bearing the P23H mutation salubrinal treatment caused a significant reduction of activated Aif in the retina but not of activated calpains. The different effect on Aif and on calpains can be explained by the fact that Aif can be activated by several proteases and among those caspases (43, 44). Activation of caspases in retinas with dominant mutations in Rho have been previously reported (23, 24, 33, 42, 45–47) and is also suggested by our analyses of cleavage of the cytoskeletal protein αII-spectrin that revealed lower molecular weight fragments in P23H mutant retinas, not observed in the retina with Rho loss of function.

The expression of a dominant mutation in Rho activates additional pathways involving ER-stress. Mutations in integral membrane proteins affecting folding cause ER retention and are linked to diseases, as also shown for Rho (48, 49). Correlation of the ER-stress Perk pathway with intracellular Ca^{2+} variations and with calpains was previously described in retina and brain neurons but not well characterized (50–54). By treatment with drugs targeting either calpains or ER-stress, we determined that these are parallel pathways. In fact, treatment with calpastatin did not significantly affect phosphorylation of ER-stress sensors. Similarly, treatment with salubrinal did not reduce the number of cells activating calpains but nearly increased calpain activity even in the presence of calpastatin. Salubrinal was reported to only moderately reduce calpain activity when a cancer cell line was pretreated with salubrinal before activation of calpains and to increase cytosolic Ca^{2+} in EBV-transformed B cells (55, 56). If indeed salubrinal increases cytosolic Ca^{2+} in photoreceptors as well, this may activate several calpains and not only calpain 1 and 2. Calpastatin specifically blocks calpain 1 and 2 that we previously demonstrated to be linked to photoreceptor cell death (27). Interfering with the two pathways in co-treatment experiments showed a significant benefit when compared to single treatments confirming that calpains and ER-stress are independently activated. Our study thus highlights the

importance of combined treatments of dominant RP caused by mutations in the *RHO* gene. Neuroprotective effects with salubrinal are consistent with the beneficial effects observed in photoreceptors from a patient bearing a dominant RHO mutation (E181K) (57). Interestingly, in our studies salubrinal not only increased phosphorylated Eif2α but also maintained activation of Ire1. Sustained expression of activated Ire1 was previously shown to have protective effects in *Drosophila* on photoreceptors expressing mutant Rho (58). Salubrinal was also previously reported to protect cells from the deleterious effect of ER-stress in a *Drosophila* model of retinal degeneration (59).

Activation of ER-stress is consistent with the observation of high molecular weight Rho protein in retinal extracts from mice expressing the dominant mutation. We also observed a different distribution of the protein in the photoreceptor cells. These data are partially discordant with a study of the knock-in mouse expressing two P23H mutant alleles (28). The apparent discrepancy may be due to the different genotypes of the mice used in the two studies. In fact, in this study we analyzed mice bearing a single mutant allele in the absence of the wild type allele while the published study analyzed mice with two P23H mutant alleles. A second explanation may reside with the methods used here for epitope retrieval in immunofluorescence experiments and for protein extraction in immunoblotting. In fact, different detergents were reported to affect the Rho pattern during immunoblotting (60).

Recessive mutations are rare in the *RHO* gene and the only confirmed null mutation is the E249X mutation identified in one patient (4). The loss of function effects of the second mutation, E150K, found in homozygosity in patients is still controversial because molecular and functional studies in the recently generated knock-in mouse identify this mutation as a slowly progressing adRP (61).

In summary, our study demonstrates that dominant and recessive mutations in the *Rho* gene trigger different responses in photoreceptor cells. While clinical symptoms are similar in patients with adRP and arRP, RP caused by the P23H mutation is not due to haploinsufficiency, and therapeutic strategies will need to account for the different molecular events triggered by different mutations. Our study only assessed the effects of calpastatin peptide and salubrinal on the retina after 16 hours of exposure analyzing the number of $TUNEL^{+}$ cells and activation of the pathways, these experiments are therefore not appropriate to evaluate preservation of the number and morphology of rod and cone photoreceptors. Long-term effects of these drugs in the eye as well as neuroprotective activities need to be evaluated for their therapeutic use in retinal degeneration. Treatments *in vivo* with salubrinal or continuous expression of calpastatin in the forebrain of transgenic mice did not show adverse effects, but long-term exposure in the eye was not assessed (62–66). The identification of the two cell death pathways paves the way for specific pharmacological screenings to identify new, safe and effective drugs for the treatment of this blinding disease.

Materials and Methods

Animal care

All procedures on mice were conducted at CSSI (Centro Servizi Stabulario Interdipartimentale) and approved by the Ethical Committee of University of Modena and Reggio Emilia (Prot. N. 106 22/11/2012) and by the Italian Ministero della Salute (346/2015-PR). Rhodopsin P23H transgenic mice (*P23H*^{Tg}) (14) were kindly provided by M. Humphries and T. Dryja and bred on a C57BL/6J genetic background, C57BL/6J wild-type mice were purchased from Envigo Italy (Udine, IT). We chose to maintain the endogenous murine Rho in this model because, in the absence of endogenous Rho, retinal degeneration proceeds rapidly affecting our analyses. *Rho*$^{-/-}$ mice in a 129/sv background (26) were kindly provided by M. Humphries. The P23H knock-in mice in a C57BL/6J background (17) were mated with the Rho knock-out mice to obtain mice with one Rho null allele and one P23H mutant Rho allele (*Rho*$^{P23H/-}$). Mice were maintained in a 12hr light/dark cycle and had free access to food and water.

In vivo treatments

For intravitreal administration, mice at the age of 9 days after birth (PN9) or PN15 or PN44 were anesthetized with an intraperitoneal injection of 250 mg/kg body weight of avertin (1.25% (w/v) 2,2,2-tribromoethanol and 2.5% (v/v) 2-methyl-2-butanol; Sigma, Milan, IT). Subsequently, the eyelid was opened and a 34GA needle was inserted adjacent to the limbal border of the cornea. 0.5 μl of calpastatin peptide (200 μM solution, with an expected final concentration in the eye of 20 μM; Calbiochem, Milan, IT) were delivered intravitreously and the control eyes received vehicle only (PBS). Salubrinal was injected twice per day intraperitoneally starting at the age of PN7 (50 μl of a 1:50 dilution in 0.9%

NaCl of a 5 mg/ml stock solution in DMSO; Calbiochem). Control mice received the same volume of vehicle (2% DMSO in 0.9% NaCl).

Calpain activity assay

Cryosections from unfixed retinas were incubated for 15 min in calpain reaction buffer (CRB: 25 mM HEPES-KOH pH 7.2, 65 mM KCl, 2 mM $MgCl_2$, 1.5 mM $CaCl_2$, 2 mM DTT) and then exposed for 1 h at 37°C to the fluorescent calpain substrate CMAC, t-BOC-Leu-Met (A6520, Life Technologies, Monza, IT) at a final concentration of 2 μM as in (20). Slides were analyzed at an Axioskop 40 fluorescence microscope (Zeiss, Arese, IT) using the filter excitation/emission wavelengths of 365/420 nm.

DNA Nick-End Labeling by TUNEL and immunofluorescence

Eyes were oriented, fixed in Davidson's fixative (8% Formaldehyde, 31.5% Ethanol, 2 M Acetic Acid), embedded in paraffin and 5 μm sections along the superior-inferior axis were collected. Apoptotic nuclei were detected by TdT-mediated dUTP terminal nick-end labeling kit (TUNEL, fluorescein; Roche, Milan, IT) used according to the manufacturer's protocols. Sections were boiled with 10 mM Tris-HCl pH 9, incubated at 60°C for 10 min and at room temperature for 30 min. Primary antibodies were employed as follows: anti-Aif (1:100; Sigma), anti-Perk (1:50, H-300: sc-13073, Santa Cruz Biotechnology), anti-phosphorylated Ire1 (1:100, Novus Biologicals, Milan, IT), anti-phosphorylated Perk (1:100, Cell Signaling), anti-Rho (1:1000, 1D4; Sigma). Secondary antibodies were Oregon Green® 488 anti-mouse, Alexa Fluor® 568 anti-mouse, anti-goat and anti-rabbit antibodies (Life Technologies). Slides were mounted with mowiol 4-88 (Sigma) and analyzed with an Axioskop 40 fluorescence microscope (Zeiss). Quantification of labeled cells was

performed by counting all labeled cells in the photoreceptor cell layer passing through the optic nerve in at least 3 sections from different animals.

Cytofluorimetric analysis of calcium

Intracellular calcium levels were determined with the intracellular calcium probe Fluo-4 AM (Life Technologies). Retinas were incubated in 19 U/ml papain for 30 min and, after 33-fold dilution with DMEM containing 10 U/ml DNAse, retina cells were dissociated by trituration. After three washes with PBS, cells were incubated with Fluo-4 AM at 37°C for 30 min in Ca^{2+}-free medium. Fluorescence was measured with a Coulter Epics XL-MCL flow cytometer (Beckman Coulter) at an excitation wavelength of 488nm. Photoreceptor cells stained with anti-Rho antibody 1D4 (1:1000, Sigma) had been previously characterized as in (67) and plotted over the forward scatter to define the gating strategy for the following intracellular calcium analysis (see Figure S2 A). Fluo4 AM signal was measured at PN10 for $P23H^{Tg}$, PN16 for $Rho^{P23H/-}$ and PN45 for $Rho^{-/-}$ in at least three different retinas and the percentages of cells with high fluorescence were compared to the age-matched wild type controls.

RT-PCR

Total RNA was extracted from murine retinas with Trizol (Life Technologies) and cDNA was synthesized using the Transcriptor High Fidelity cDNA Synthesis Kit (Roche). PCR analysis of the spliced form of *Xbp1* was performed with primers specifically recognizing the spliced variant (sXbp1-f: GGTCTGCTGAGTCCGCAGCAGG and sXbp1-r: CAGGCCTATGCTATCCTCTAGGC) with the following protocol: 10 min at 95°C followed by 30 cycles composed by 30 sec at 95°C, 30 sec at 64°C and 90 sec at 72°C. The

expected PCR product consisted of 718 bp. PCR was normalized with primers for the *S26* gene (S26-f: AAGTTTGTCATTCGGAACATT and S26-r: GATCGATTCCTAACAACCTTG).

Retinal protein extracts and Western blotting analysis

Retinas were dissected in PBS. Total cell extracts were prepared by homogenizing retinas in 20 mM Tris-HCl pH 7.4, 150 mM NaCl, 1% CHAPS, 0.2 mM Na_3PO_4, 1 mM Na_3VO_4, protease inhibitor cocktail (Sigma) and centrifugation at 17000xg for 10 min. For nuclei-enriched lysate preparation, retinas were transferred into a 2 ml Dounce homogenizer with 200 µl of cold homogenizing buffer (20 mM HEPES-KOH pH 7.5, 250 mM sucrose, 10 mM KCl, 1.5 mM $MgCl_2$, 2 mM EDTA, 1 mM DTT, 0.2 mM Na_3PO_4, 1 mM Na_3VO_4, protease inhibitor cocktail from Sigma) and placed on ice for 30 min. The tissue was disrupted with 40 strokes and centrifuged at 900xg for 5 min at 4°C to isolate the nuclear fraction. The pellet was washed twice in cold homogenizing buffer and resuspended in lysis buffer (50 mM Tris-HCl pH 7.4, 150 mM NaCl, 1% NP-40, 0.1% SDS, 1 mM EDTA, 0.2 mM Na_3PO_4, 1 mM Na_3VO_4, protease inhibitor cocktail from Sigma). The purity of enriched lysates was checked by western blotting with a nuclear marker (anti-Histone H3 1:3000; Bethyl Laboratories, Bologna, IT) and a cytosol marker (anti-pan-actin, 1:3000, Millipore).

Equivalent amounts of protein extracts (3 µg for total extracts, 20 µg for nuclear extracts and 80 µg for analyses of αII-spectrin) were resolved using SDS-PAGE and immunoblottings were performed following standard procedures. The antibodies used for immunoblotting were: anti-Aif (1:1000; Oncogene), anti-αII-spectrin (anti-fodrin; 1:2000, Enzo Life, Roma, IT), anti-Bip (1:1000, Santa Cruz Biotechnology), anti-Eif2α (1:1000, Cell Signaling), anti-Histone H3 (1:3000; Bethyl Laboratories), anti-phosphorylated-Ire1 (1:2000, Novus Biologicals), anti-phosphorylated-Perk (1:1000, Cell Signaling), anti-phosphorylated-Eif2α (1:1000, Cell Signaling), anti-Perk (1:1000, Santa Cruz

Biotechnology), anti-pan-actin (1:3000, Millipore), and anti-recoverin (1:1000, Millipore). Quantification was performed by densitometry analysis of scanned images with ImageJ software, corrected for background and plotted as protein/normalizing protein. Data are presented as means ± SD of 3 blots with proteins derived as biological replicates from 3 animals.

Statistical analysis

Cell counts and densitometry analyses are shown as means ± SD. Paired Student's t-test analysis was performed to compare data derived from at least three different wild-type or mock treated mutant retinas to at least three different mutant or drug treated retinas, respectively.

Acknowledgments

Authors would like to thank Alessandra Recchia and Francesca Fanelli for helpful discussion. We acknowledge the CIGS (Cinzia Restani) and CSSI of University of Modena and Reggio Emilia for providing confocal microscopy and animal husbandry assistance as well as the Cell-lab facility at University of Modena and Reggio Emilia. K.P. is the John H. Hord Professor of Pharmacology. This work was supported by research grant GGP11201A from Fondazione Telethon, E-RARE 2009 RHORCOD; by Programma di ricerca Regione-Università 2010-2012 of Regione Emilia Romagna (RARER); by research grant of Fondazione Roma (call for proposal 2013 sulla Retinite Pigmentosa); The Arnold and Mabel Beckman Foundation; and Foundation Fighting Blindness.

Conflict of interest disclosure

None.

References

1. Hartong,D.T., Berson,E.L. and Dryja,T.P. (2006) Retinitis pigmentosa. *Lancet*, **368**, 1795–1809.
2. Trifunović,D., Karali,M., Camposampiero,D., Ponzin,D., Banfi,S. and Marigo,V. (2008) A high-resolution RNA expression atlas of retinitis pigmentosa genes in human and mouse retinas. *Invest Ophthalmol Vis Sci*, **49**, 2330–2336.
3. Kumaramanickavel,G., Maw,M., Denton,M.J., John,S., Srikumari,C.R., Orth,U., Oehlmann,R. and Gal,A. (1994) Missense rhodopsin mutation in a family with recessive RP. *Nat Genet*, **8**, 10–11.
4. Rosenfeld,P.J., Cowley,G.S., McGee,T.L., Sandberg,M.A., Berson,E.L. and Dryja,T.P. (1992) A null mutation in the rhodopsin gene causes rod photoreceptor dysfunction and autosomal recessive retinitis pigmentosa. *Nat Genet*, **1**, 209–213.
5. Filipek,S., Stenkamp,R.E., Teller,D.C. and Palczewski,K. (2003) G protein-coupled receptor rhodopsin: a prospectus. *Annu Rev Physiol*, **65**, 851–879.
6. Hargrave,P.A. (2001) Rhodopsin structure, function, and topography the Friedenwald lecture. *Invest Ophthalmol Vis Sci*, **42**, 3–9.
7. Palczewski,K. (2006) G protein-coupled receptor rhodopsin. *Ann Rev Biochem*, **75**, 743–767.
8. Lin,J.H., Li,H., Yasumura,D., Cohen,H.R., Zhang,C., Panning,B., Shokat,K.M., LaVail,M.M. and Walter,P. (2007) IRE1 signaling affects cell fate during the unfolded protein response. *Science (80-.).*, **318**, 944–949.
9. Frederick,J.M., Krasnoperova,N. V, Hoffmann,K., Church-Kopish,J., Ruther,K., Howes,K., Lem,J. and Baehr,W. (2001) Mutant rhodopsin transgene expression on a null background. *Invest Ophthalmol Vis Sci*, **42**, 826–833.
10. Griciuc,A., Aron,L. and Ueffing,M. (2011) ER stress in retinal degeneration: a target for rational therapy? *Trends Mol Med*, **17**, 442–451.
11. Griciuc,A., Aron,L., Piccoli,G. and Ueffing,M. (2010) Clearance of Rhodopsin(P23H) aggregates requires the ERAD effector VCP. *Biochim Biophys Acta*, **1803**, 424–434.
12. Dryja,T.P., McGee,T.L., Hahn,L.B., Cowley,G.S., Olsson,J.E., Reichel,E., Sandberg,M.A. and Berson,E.L. (1990) Mutations within the rhodopsin gene in patients with autosomal dominant retinitis pigmentosa. *N Engl J Med*, **323**, 1302–1307.
13. Saliba,R.S., Munro,P.M.G., Luthert,P.J. and Cheetham,M.E. (2002) The cellular fate of mutant rhodopsin: quality control, degradation and aggresome formation. *J Cell Sci*, **115**, 2907–2918.
14. Olsson,J.E., Gordon,J.W., Pawlyk,B.S., Roof,D., Hayes,A., Molday,R.S., Mukai,S., Cowley,G.S., Berson,E.L. and Dryja,T.P. (1992) Transgenic mice with a rhodopsin mutation (Pro23His): a mouse model of autosomal dominant retinitis pigmentosa. *Neuron*, **9**, 815–830.
15. Machida,S., Kondo,M., Jamison,J.A., Khan,N.W., Kononen,L.T., Sugawara,T., Bush,R.A. and Sieving,P.A. (2000) P23H rhodopsin transgenic rat: correlation of retinal function with histopathology. *Invest Ophthalmol Vis Sci*, **41**, 3200–3209.
16. Price,B.A., Sandoval,I.M., Chan,F., Simons,D.L., Wu,S.M., Wensel,T.G. and Wilson,J.H. (2011) Mislocalization and Degradation of Human P23H-Rhodopsin-GFP

in a Knockin Mouse Model of Retinitis Pigmentosa. *Invest Ophthalmol Vis Sci*, **52**, 9728–9736.

17. Sakami,S., Maeda,T., Bereta,G., Okano,K., Golczak,M., Sumaroka,A., Roman,A.J., Cideciyan,A. V, Jacobson,S.G. and Palczewski,K. (2011) Probing mechanisms of photoreceptor degeneration in a new mouse model of the common form of autosomal dominant retinitis pigmentosa due to P23H opsin mutations. *J Biol Chem*, **286**, 10551–10567.
18. Wang,M. and Kaufman,R.J. (2016) Protein misfolding in the endoplasmic reticulum as a conduit to human disease. *Nature*, **529**, 326–335.
19. Sanges,D., Comitato,A., Tammaro,R. and Marigo,V. (2006) Apoptosis in retinal degeneration involves cross-talk between apoptosis-inducing factor (AIF) and caspase-12 and is blocked by calpain inhibitors. *Proc Natl Acad Sci USA*, **103**, 17366–17371.
20. Paquet-Durand,F., Sanges,D., McCall,J., Silva,J., van Veen,T., Marigo,V. and Ekström,P. (2010) Photoreceptor rescue and toxicity induced by different calpain inhibitors. *J Neurochem*, **115**, 930–940.
21. Cande,C., Vahsen,N., Kouranti,I., Schmitt,E., Daugas,E., Spahr,C., Luban,J., Kroemer,R.T., Giordanetto,F., Garrido,C., *et al.* (2004) AIF and cyclophilin A cooperate in apoptosis-associated chromatinolysis. *Oncogene*, **23**, 1514–1521.
22. Moubarak,R.S., Yuste,V.J., Greer,P.A., Artus,C., Bouharrour,A., Menissier-de Murcia,J. and Susin,S.A. (2007) Sequential activation of poly(ADP-ribose) polymerase 1, calpains, and Bax is essential in apoptosis-inducing factor-mediated programmed necrosis. *Mol Cell Biol*, **27**, 4844–4862.
23. Gorbatyuk,M.S., Knox,T., LaVail,M.M., Gorbatyuk,O.S., Noorwez,S.M., Hauswirth,W.W., Lin,J.H., Muzyczka,N. and Lewin,A.S. (2010) Restoration of visual function in P23H rhodopsin transgenic rats by gene delivery of BiP/Grp78. *Proc Natl Acad Sci USA*, **107**, 5961–5966.
24. Sizova,O.S., Shinde,V.M., Lenox,A. and Gorbatyuk,M.S. (2014) Modulation of cellular signaling pathways in P23H rhodopsin photoreceptors. *Cell Signal*, **26**, 665–672.
25. Ozaki,T., Ishiguro,S., Hirano,S., Baba,A., Yamashita,T., Tomita,H. and Nakazawa,M. (2013) Inhibitory peptide of mitochondrial μ-calpain protects against photoreceptor degeneration in rhodopsin transgenic S334ter and P23H rats. *PLoS One*, **8**, e71650.
26. Humphries,M.M., Rancourt,D., Farrar,G.J., Kenna,P., Hazel,M., Bush,R.A., Sieving,P.A., Sheils,D.M., McNally,N., Creighton,P., *et al.* (1997) Retinopathy induced in mice by targeted disruption of the rhodopsin gene. *Nat Genet*, **15**, 216–219.
27. Comitato,A., Sanges,D., Rossi,A., Humphries,M.M. and Marigo,V. (2014) Activation of Bax in Three Models of Retinitis Pigmentosa. *Invest Ophthalmol Vis Sci*, **55**, 3555–3562.
28. Chiang,W.-C., Kroeger,H., Sakami,S., Messah,C., Yasumura,D., Matthes,M.T., Coppinger,J.A., Palczewski,K., LaVail,M.M. and Lin,J.H. (2015) Robust Endoplasmic Reticulum-Associated Degradation of Rhodopsin Precedes Retinal Degeneration. *Mol Neurobiol*, **52**, 679–695.
29. Colley,N.J., Cassill,J.A., Baker,E.K. and Zuker,C.S. (1995) Defective intracellular transport is the molecular basis of rhodopsin-dependent dominant retinal degeneration. *Proc Natl Acad Sci USA*, **92**, 3070–3074.

30. Mendes,H.F. and Cheetham,M.E. (2008) Pharmacological manipulation of gain-of-function and dominant-negative mechanisms in rhodopsin retinitis pigmentosa. *Hum Mol Genet*, **17**, 3043–3054.

31. Parfitt,D.A., Aguila,M., McCulley,C.H., Bevilacqua,D., Mendes,H.F., Athanasiou,D., Novoselov,S.S., Kanuga,N., Munro,P.M., Coffey,P.J., *et al.* (2014) The heat-shock response co-inducer arimoclomol protects against retinal degeneration in rhodopsin retinitis pigmentosa. *Cell Death Dis*, **5**, e1236.

32. Arango-Gonzalez,B., Trifunović,D., Sahaboglu,A., Kranz,K., Michalakis,S., Farinelli,P., Koch,S., Koch,F., Cottet,S., Janssen-Bienhold,U., *et al.* (2014) Identification of a common non-apoptotic cell death mechanism in hereditary retinal degeneration. *PLoS One*, **9**, e112142.

33. Kaur,J., Mencl,S., Sahaboglu,A., Farinelli,P., van Veen,T., Zrenner,E., Ekström,P.A., Paquet-Durand,F. and Arango-Gonzalez,B. (2011) Calpain and PARP activation during photoreceptor cell death in P23H and S334ter rhodopsin mutant rats. *PLoS One*, **6**, e22181.

34. Doonan,F., Donovan,M. and Cotter,T.G. (2005) Activation of Multiple Pathways during Photoreceptor Apoptosis in the rd Mouse. *Invest Ophthalmol Vis Sci*, **46**, 3530–3538.

35. Kroeger,H., Messah,C., Ahern,K., Gee,J., Joseph,V., Matthes,M.T., Yasumura,D., Gorbatyuk,M.S., Chiang,W.-C., LaVail,M.M., *et al.* (2012) Induction of Endoplasmic Reticulum Stress Genes, BiP and Chop, in Genetic and Environmental Models of Retinal Degeneration. *Invest Ophthalmol Vis Sci*, **53**, 7590–7599.

36. Boyce,M., Bryant,K.F., Jousse,C., Long,K., Harding,H.P., Scheuner,D., Kaufman,R.J., Ma,D., Coen,D.M., Ron,D., *et al.* (2005) A selective inhibitor of eIF2alpha dephosphorylation protects cells from ER stress. *Science (80-.).*, **307**, 935–939.

37. Sancho-Pelluz,J., Arango-Gonzalez,B., Kustermann,S., Romero,F.J., van Veen,T., Zrenner,E., Ekström,P. and Paquet-Durand,F. (2008) Photoreceptor cell death mechanisms in inherited retinal degeneration. *Mol Neurobiol*, **38**, 253–269.

38. Paquet-Durand,F., Azadi,S., Hauck,S.M., Ueffing,M., van Veen,T. and Ekström,P. (2006) Calpain is activated in degenerating photoreceptors in the rd1 mouse. *J Neurochem*, **96**, 802–814.

39. Trifunović,D., Dengler,K., Michalakis,S., Zrenner,E., Wissinger,B. and Paquet-Durand,F. (2010) cGMP-dependent cone photoreceptor degeneration in the cpfl1 mouse retina. *J Comp Neurol*, **518**, 3604–3617.

40. Sothilingam,V., Garcia Garrido,M., Jiao,K., Buena-Atienza,E., Sahaboglu,A., Trifunović,D., Balendran,S., Koepfli,T., Mühlfriedel,R., Schön,C., *et al.* (2015) Retinitis pigmentosa: impact of different Pde6a point mutations on the disease phenotype. *Hum Mol Genet*, **24**, 5486–5499.

41. Marigo,V. (2007) Programmed Cell Death in Retinal Degeneration. *Cell Cycle*, **6**, 652–655.

42. Marsili,S., Genini,S., Sudharsan,R., Gingrich,J., Aguirre,G.D. and Beltran,W.A. (2015) Exclusion of the unfolded protein response in light-induced retinal degeneration in the canine T4R RHO model of autosomal dominant retinitis pigmentosa. *PLoS One*, **10**, e0115723.

43. Lakhani,S.A., Masud,A., Kuida,K., Porter Jr.,G.A., Booth,C.J., Mehal,W.Z., Inayat,I. and Flavell,R.A. (2006) Caspases 3 and 7: key mediators of mitochondrial events of

apoptosis. *Science (80-.).*, **311**, 847–851.

44. Arnoult,D., Gaume,B., Karbowski,M., Sharpe,J.C., Cecconi,F. and Youle,R.J. (2003) Mitochondrial release of AIF and EndoG requires caspase activation downstream of Bax/Bak-mediated permeabilization. *Embo J*, **22**, 4385–4399.
45. Samardzija,M., Wenzel,A., Thiersch,M., Frigg,R., Remé,C. and Grimm,C. (2006) Caspase-1 Ablation Protects Photoreceptors in a Model of Autosomal Dominant Retinitis Pigmentosa. *Invest Ophthalmol Vis Sci*, **47**, 5181–5190.
46. Liu,C., Li,Y., Peng,M., Laties,A.M. and Wen,R. (1999) Activation of caspase-3 in the retina of transgenic rats with the rhodopsin mutation s334ter during photoreceptor degeneration. *J Neurosci*, **19**, 4778–4785.
47. Zeiss,C.J., Neal,J. and Johnson,E.A. (2004) Caspase-3 in postnatal retinal development and degeneration. *Invest Ophthalmol Vis Sci*, **45**, 964–970.
48. Castro-Fernández,C., Maya-Núñez,G. and Conn,P.M. (2005) Beyond the signal sequence: protein routing in health and disease. *Endocr Rev*, **26**, 479–503.
49. Mendes,H.F., van der Spuy,J., Chapple,J.P. and Cheetham,M.E. (2005) Mechanisms of cell death in rhodopsin retinitis pigmentosa: implications for therapy. *Trends Mol Med*, **11**, 177–185.
50. Badiola,N., Penas,C., Miñano-Molina,A., Barneda-Zahonero,B., Fadó,R., Sánchez-Opazo,G., Comella,J.X., Sabriá,J., Zhu,C., Blomgren,K., *et al.* (2011) Induction of ER stress in response to oxygen-glucose deprivation of cortical cultures involves the activation of the PERK and IRE-1 pathways and of caspase-12. *Cell Death Dis*, **2**, e149.
51. Han,G., Casson,R.J., Chidlow,G. and Wood,J.P.M. (2014) The Mitochondrial Complex I Inhibitor Rotenone Induces Endoplasmic Reticulum Stress and Activation of GSK-3β in Cultured Rat Retinal Cells. *Invest Ophthalmol Vis Sci*, **55**, 5616–5628.
52. Janyou,A., Changtam,C., Suksamrarn,A., Tocharus,C. and Tocharus,J. (2015) Suppression effects of O-demethyldemethoxycurcumin on thapsigargin triggered on endoplasmic reticulum stress in SK-N-SH cells. *Neurotoxicology*, **50**, 92–100.
53. Lu,T.-H., Su,C.-C., Tang,F.-C., Chen,C.-H., Yen,C.-C., Fang,K.-M., Lee,K.-I., Hung,D.-Z. and Chen,Y.-W. (2015) Chloroacetic acid triggers apoptosis in neuronal cells via a reactive oxygen species-induced endoplasmic reticulum stress signaling pathway. *Chem Biol Interact*, **225**, 1–12.
54. de la Cadena,S.G., Hernández-Fonseca,K., Camacho-Arroyo,I. and Massieu,L. (2014) Glucose deprivation induces reticulum stress by the PERK pathway and caspase-7- and calpain-mediated caspase-12 activation. *Apoptosis*, **19**, 414–427.
55. Park,G. Bin, Kim,Y.S., Lee,H.-K., Song,H., Kim,S., Cho,D.-H. and Hur,D.Y. (2011) Reactive oxygen species and p38 MAPK regulate Bax translocation and calcium redistribution in salubrinal-induced apoptosis of EBV-transformed B cells. *Cancer Lett*, **313**, 235–248.
56. Yang,W., Tiffany-Castiglioni,E., Koh,H.C. and Son,I.-H. (2009) Paraquat activates the IRE1/ASK1/JNK cascade associated with apoptosis in human neuroblastoma SH-SY5Y cells. *Toxicol Lett*, **191**, 203–210.
57. Yoshida,T., Ozawa,Y., Suzuki,K., Yuki,K., Ohyama,M., Akamatsu,W., Matsuzaki,Y., Shimmura,S., Mitani,K., Tsubota,K., *et al.* (2014) The use of induced pluripotent stem cells to reveal pathogenic gene mutations and explore treatments for retinitis

pigmentosa. *Mol Brain*, **7**, 45.

58. Griciuc,A., Aron,L., Roux,M.J., Klein,R., Giangrande,A. and Ueffing,M. (2010) Inactivation of VCP/ ter94 Suppresses Retinal Pathology Caused by Misfolded Rhodopsin in Drosophila. *PLoS Genet*, **6**, e1001075.
59. Mendes,C.S., Levet,C., Chatelain,G., Dourlen,P., Fouillet,A., Dichtel-Danjoy,M.-L., Gambis,A., Ryoo,H.D., Steller,H. and Mollereau,B. (2009) ER stress protects from retinal degeneration. *Embo J*, **28**, 1296–1307.
60. Jastrzebska,B., Maeda,T., Zhu,L., Fotiadis,D., Filipek,S., Engel,A., Stenkamp,R.E. and Palczewski,K. (2004) Functional characterization of rhodopsin monomers and dimers in detergents. *J Biol Chem*, **279**, 54663–54675.
61. Zhang,N., Kolesnikov,A. V, Jastrzebska,B., Mustafi,D., Sawada,O., Maeda,T., Genoud,C., Engel,A., Kefalov,V.J. and Palczewski,K. (2013) Autosomal recessive retinitis pigmentosa E150K opsin mice exhibit photoreceptor disorganization. *J Clin Invest*, **123**, 121–137.
62. Hamamura,K., Nishimura,A., Iino,T., Takigawa,S., Sudo,A. and Yokota,H. (2015) Chondroprotective effects of Salubrinal in a mouse model of osteoarthritis. *Bone Jt. Res*, **4**, 84–92.
63. Huang,X., Chen,Y., Zhang,H., Ma,Q., Zhang,Y. and Xu,H. (2012) Salubrinal attenuates β-amyloid-induced neuronal death and microglial activation by inhibition of the NF-κB pathway. *Neurobiol Aging*, **33**, 1007.e9–1007.e17.
64. Higuchi,M., Tomioka,M., Takano,J., Shirotani,K., Iwata,N., Masumoto,H., Maki,M., Itohara,S. and Saido,T.C. (2005) Distinct mechanistic roles of calpain and caspase activation in neurodegeneration as revealed in mice overexpressing their specific inhibitors. *J Biol Chem*, **280**, 15229–15237.
65. Rubovitch,V., Barak,S., Rachmany,L., Goldstein,R.B., Zilberstein,Y. and Pick,C.G. (2015) The neuroprotective effect of salubrinal in a mouse model of traumatic brain injury. *Neuromol Med*, **17**, 58–70.
66. Sokka,A.-L., Putkonen,N., Mudo,G., Pryazhnikov,E., Reijonen,S., Khiroug,L., Belluardo,N., Lindholm,D. and Korhonen,L. (2007) Endoplasmic reticulum stress inhibition protects against excitotoxic neuronal injury in the rat brain. *J Neurosci*, **27**, 901–908.
67. Portillo,J.-A.C., Okenka,G., Kern,T.S. and Subauste,C.S. (2009) Identification of primary retinal cells and ex vivo detection of proinflammatory molecules using flow cytometry. *Mol Vis*, **15**, 1383–1389.

Legends to figures

Figure 1. Calpain and Aif activation in retinas bearing mutation in the *Rho* gene. (**A**) Immunoblot of total protein extracts (PN9 for $Rho^{+/+}$ and $P23H^{Tg}$; PN16 for $Rho^{+/-}$ and $Rho^{P23H/-}$; PN45 for $Rho^{+/+}$ and $Rho^{-/-}$) with an anti-αII-spectrin antibody is shown. All mutant retinas manifest an increased intensity of the 145 kDa band (arrow). Retinas expressing the P23H mutation also show fragments of αII-spectrin at 120 kDa (asterisk) consistent with activation of caspases. The immunoblot was normalized with anti-actin antibodies (lower panel). MW: molecular weight markers are shown in kDa. (**B**) Histogram representing the percentages of cells co-labeled with TUNEL and with the calpain activity assay. (**C**) Confocal images showing co-localization (yellow, arrows) of Aif (red) and TUNEL (green) inside nuclei of $P23H^{Tg}$ retinas at PN9, $Rho^{P23H/-}$ retinas at PN16, and $Rho^{-/-}$ retinas at PN45. IS = inner segment (containing photoreceptor cytoplasm and mitochondria); ONL= outer nuclear layer; INL = inner nuclear layer. Scale bar: 50μm (**D**) Histogram representing percentages of cells co-labeled with TUNEL and with the anti-Aif antibody. (**E**) Immunoblots of nuclear enriched extracts from $Rho^{+/+}$ PN10 and $P23H^{Tg}$ retinas at PN8, PN9 and PN10 (8, 9 10 in the figure), from $Rho^{+/-}$ PN20 and $Rho^{P23H/-}$ retinas at PN12, PN16 and PN20 (12, 16, 20 in the figure), from $Rho^{+/+}$ PN30 and $Rho^{-/-}$ retinas at PN30, PN45 and PN60 (30, 45, 60 in the figure) using an anti-Aif antibody. Immunoblots were normalized with anti-histone H3 antibodies (lower panels). MW: molecular weight markers are shown in kDa.

Figure 2. Neuroprotective effects of calpastin peptide treatment. (**A**) Total protein extracts from mouse retinas were analyzed by immunoblot at the age of PN10 for $P23H^{Tg}$, PN16 for $Rho^{P23H/-}$ and PN45 for $Rho^{-/-}$ with an anti-αII-spectrin antibody and in age-matched controls ($Rho^{+/+}$ PN10; $Rho^{+/-}$ PN16; $Rho^{+/+}$ PN45). The reduction of the 145 kDa

fragment resulting from calpain cleavage (arrow) in calpastatin peptide (CS) treated retinas when compared to vehicle treated control retinas (mock) confirmed the inhibition of calpain activation by CS. The immunoblot was normalized with anti-actin antibodies (lower panel). MW: molecular weight markers are shown in kDa. (**B**) Histogram with percentages of photoreceptors co-labeled with TUNEL and the calpain activity assay, as detected *in situ* with a fluorescent calpain substrate, indicates a significant reduction of dying cells activating calpains after treatment with CS in all models. (**C**) Immunoblot of nuclear protein extracts shows reduced nuclear translocation of Aif in CS treated samples. The immunoblot was normalized with anti-Histone H3 antibodies (lower panel). MW: molecular weight markers are shown in kDa. (**D**) Histogram with percentages of photoreceptors co-labeled with TUNEL and nuclear localized Aif reveals a reduction of dying cells activating Aif after treatment with CS in all models. (**E**) Histogram with percentages of TUNEL-labeled photoreceptors shows a reduction of photoreceptor cell death after treatment with CS. *** $P \leq 0.001$; * $P \leq 0.05$ Student's t-test comparing treated retinas (white bars) with the corresponding mock treated controls (gray bars).

Figure 3. Time course of ER-stress activation in P23H^{Tg}. Ire1 and Perk pathway activations were analyzed in *Rho*$^{+/+}$ and *P23H*^{Tg} retinas at PN8, PN9 and PN10 (8, 9 10 in figure). (**A**) Immunoblot of total protein extracts shows phosphorylation/activation of Ire1 (phospho-Ire1 antibody) in the mutant retina at PN8, PN9 and PN10, the last at a reduced level. The immunoblot was normalized using anti-actin antibodies (lower panel). MW: molecular weight markers are shown in kDa. (**B**) RT-PCR with primers specific for the spliced form of *Xbp1* (*sXbp1*) confirmed activation of the Ire1 pathway in PN8 and PN9 mutant retinas. RT-PCR was normalized with primers specific for *S26*. MW=molecular weight marker showing DNA fragments every 100 bp starting from the lower band at 100 bp. (**C**) Immunofluorescence analysis of retinas at PN9 with anti-phospho-Ire antibodies

(red in the inner segment, containing the cytoplasm of photoreceptor cells, is indicated by an arrow) confirmed activation of the Ire1 pathway in the photoreceptor cells also labeled by TUNEL (green). Nuclei are stained with DAPI (blue). Scale bar: 20μm. (**D**) Immunoblot of total protein extracts shows phosphorylation/activation of Perk (phospho-Perk antibody) in the mutant retina at all tested time points. The immunoblot was normalized using anti-Perk antibodies to visualize total Perk protein (lower panel) and to be compared to the activated-phosphorylated form shown in the upper panel. MW: molecular weight markers are shown in kDa. (**E**) Immunoblot shows phosphorylation of Eif2α in the mutant retina at all tested time points. The immunoblot was normalized using anti-Eif2α antibodies to visualize total Eif2α protein (lower panel). MW: molecular weight markers are shown in kDa. (**F**) Immunofluorescence analysis of retinas at PN10 with antibodies anti-P-Perk (red in the inner segment, containing the cytoplasm of photoreceptor cells, is indicated by an arrow) confirmed activation of the Perk pathway in the photoreceptor cells also labeled by TUNEL (green). Nuclei are stained with DAPI (blue). Scale bar: 20μm. IS = inner segment (containing photoreceptor cytoplasm and mitochondria); ONL= outer nuclear layer; INL = inner nuclear layer; GCL=ganglion cell layer.

Figure 4. Time course of ER-stress activation in Rho$^{P23H/-}$. Ire1 and Perk pathway activations were analyzed in in *Rho*$^{P23H/-}$ retinas at PN12, PN16 and PN28 (12, 16, 28 in figure) and compared to *Rho*$^{+/-}$ retinas at the same ages. (**A**) Immunoblot of total protein extracts shows phosphorylation/activation of Ire1 (phospho-Ire1 antibody) in the mutant retina at all analyzed time points. The immunoblot was normalized using anti-actin antibodies (lower panel). MW: molecular weight markers are shown in kDa. (**B**) RT-PCR with primers specific for the spliced form of *Xbp1* (*sXbp1*) confirmed activation of the Ire1

pathway in mutant retinas. RT-PCR was normalized with primers specific for *S26*. MW=molecular weight marker showing DNA fragments every 100 bp starting from the lower band at 100 bp. (**C**) Immunofluorescence analysis of retinas at PN16 with anti-phospho-Ire antibodies (red in the inner segment, containing the cytoplasm of photoreceptor cells, is indicated by an arrow) confirmed activation of the Ire1 pathway in the photoreceptor cells also labeled by TUNEL (green). Nuclei are stained with DAPI (blue). Scale bar: 20μm. (**D**) Immunoblot of total protein extracts shows phosphorylation/activation of Perk (phospho-Perk antibody) in the mutant retina at all tested time points. The immunoblot was normalized using anti-Perk antibodies to visualize total Perk protein (lower panel) and to be compared to the activated-phosphorylated form shown in the upper panel. MW: molecular weight markers are shown in kDa. (**E**) Immunoblot shows phosphorylation of Eif2α in the mutant retina at all tested time points. The immunoblot was normalized using anti-Eif2α antibodies to visualize total Eif2α protein (lower panel). MW: molecular weight markers are shown in kDa. (**F**) Immunofluorescence analysis of retinas at PN16 with antibodies anti-phospho-Perk (red in the inner segment, containing the cytoplasm of photoreceptor cells, is indicated by an arrow) confirmed activation of the Perk pathway in the photoreceptor cells also labeled by TUNEL (green). Nuclei are stained with DAPI (blue). Scale bar: 20μm. IS = inner segment (containing photoreceptor cytoplasm and mitochondria); ONL= outer nuclear layer; INL = inner nuclear layer; GCL=ganglion cell layer.

Figure 5. Neuroprotective effects of salubrinal and calpastatin treatments. Mice were treated either with salubrinal (SAL) or calpastatin peptide (CS) or with salubrinal and calpastatin peptide together (CS+SAL). Protein extracts from retinas treated with drugs or

treated with vehicle only (mock) were analyzed at the age of PN9 for *P23H*^{Tg} and PN16 for *Rho*$^{P23H/-}$. (**A-B**) Immunoblots of total protein extracts show increased phosphorylated Ire1 (upper panels) after treatment with SAL and CS+SAL in *P23H*^{Tg} (**A**) and in *Rho*$^{P23H/-}$ (**B**) retinas. No effect on Ire1 phosphorylation was observed after treatment with CS only. Immunoblots were normalized using anti-actin antibodies (lower panel). (**C-D**) RT-PCR using primers specific for the spliced form of *Xbp1* (*sXbp1*) confirms activation of the Ire1 pathway after treatment with SAL and CS+SAL in *P23H*^{Tg} (**C**) and in *Rho*$^{P23H/-}$ (**D**) retinas. No effect on *Xbp1* splicing was observed after treatment with CS only. RT-PCR reactions were normalized with primers specific for *S26*. (**E-F**) Immunoblots of total protein extracts show no significant change of phosphorylated Perk (upper panels) in *P23H*^{Tg} (**E**) and in *Rho*$^{P23H/-}$ (**F**) retinas after treatments. The immunoblots were normalized using anti-Perk antibodies (lower panels). (**G-H**) Immunoblots of total protein extracts show increased phosphorylated Eif2α (upper panels) after treatment with SAL and CS+SAL in *P23H*^{Tg} (**G**) and in *Rho*$^{P23H/-}$ (**H**) retinas. Immunoblots were normalized using anti-Eif2α antibodies (lower panel). (**I-J**) Immunoblots of nuclear protein extracts show reduced nuclear translocation of Aif (upper panels) in *P23H*^{Tg} (**I**) and in *Rho*$^{P23H/-}$ (**J**) retinas after treatments. Immunoblots were normalized using anti-Histone H3 antibodies (lower panel). (**K-L**) Immunoblots on total protein extracts show increased Bip/Grp79 (upper panels) after treatment with SAL and CS+SAL in *P23H*^{Tg} (**K**) and in *Rho*$^{P23H/-}$ (**L**) retinas. No effect on Bip/Grp79 levels was observed after treatment with CS only. Immunoblots were normalized using anti-actin antibodies (lower panel). (**M**) Graph representing the percentages of TUNEL^{+} photoreceptors in *P23H*^{Tg} (dashed bars) and in *Rho*$^{P23H/-}$ (gray bars) after treatments with either SAL or CS or CS+SAL. A significant reduction of cell death was observed in all treated retinas when compared to retinas treated with vehicle only (mock). (**N**) Graph representing the percentages of dying photoreceptors activating

calpains (Calpain activity^{+}/TUNEL^{+}) in *P23H*^{Tg} (dashed bars) and in *Rho*$^{P23H/-}$ (gray bars) after treatments with either SAL or CS or CS+SAL. A significant reduction of calpain activation in dying cells was detected in *P23H*^{Tg} and *Rho*$^{P23H/-}$ retinas only after treatments with CS when compared to retinas treated with vehicle only (mock). (**O**) Graph representing the percentages of dying photoreceptors with nuclear localized Aif (Aif^{+}/TUNEL^{+}) in *P23H*^{Tg} (dashed bars) and in *Rho*$^{P23H/-}$ (gray bars) after treatments with either SAL or CS or CS+SAL. A significant reduction of Aif activation in dying cells was detected in all treated retinas expressing P23H mutant Rho when compared to retinas treated with vehicle only (mock). *** $P \leq 0.001$; ** $P \leq 0.01$; * $P \leq 0.05$ t-Student comparing treated retinas with the corresponding mock controls. MW: molecular weight markers are shown in kDa.

Figure S1. Characterization of murine mutant Rho models. (**A**) Time course analysis of photoreceptor cell death in *P23H*^{Tg}, *Rho*$^{P23H/-}$, and *Rho*$^{-/-}$ mutant retinas by TUNEL assay. Peak of cell death was postnatal day 9 (PN9) in *P23H*^{Tg}, PN16 in *Rho*$^{P23H/-}$, and PN45 in *Rho*$^{-/-}$. (**B**) Immunoblots using anti-Rho antibody (1D4, Sigma) of total protein extracts from retinas of *Rho*$^{P23H/-}$ compared to Rho$^{+/-}$ and *Rho*$^{-/-TgP23H}$ (*P23H*^{Tg} bred with *Rho*$^{-/-}$ to analyze only the mutant transgenic allele) compared to wild type *Rho*$^{+/+}$. Rho monomers are indicated by an open arrow. Blots were normalized with an anti-recoverin antibody (lower panel, Rec), a protein expressed in photoreceptors, to take into account on-going rod cell death at the analyzed time points. MW: molecular weight markers are shown in kDa. (**C**) Confocal images of immunofluorescence analyses of *Rho*$^{+/+}$ and *P23H*^{Tg} retinas at PN10 and *Rho*$^{+/-}$ and *Rho*$^{P23H/-}$ retinas at PN16 labeled with the anti-Rho antibody (green) and TUNEL (red). Wild type Rho accumulates in the inner segment (IS) at PN10 and in the outer segment (OS) of the more mature retina at PN16 but mutant P23H accumulates intracellularly and is retained in the inner segment. Dying cells labeled with TUNEL are

detectable only in P23H expressing retinas. Scale bars: 75μm. (**D**) Analyses of calpain activity (blue) and TUNEL (red) of *Rho*$^{+/+}$ and *P23H*^{Tg} retinas at PN10, *Rho*$^{+/-}$ and *Rho*$^{P23H/-}$ retinas at PN16 and *Rho*$^{+/+}$ and *Rho*$^{-/-}$ retinas at PN45. Arrows indicate cells co-labeled by TUNEL and the calpain activity assay; arrowheads indicate cells labeled only by the calpain activity assay. OS= outer segment; IS = inner segment (containing photoreceptor cytoplasm and mitochondria); ONL= outer nuclear layer; INL = inner nuclear layer. (**E-G**) Confocal sections of *P23H*^{Tg} (**E**), *Rho*$^{P23H/-}$ (**F**) and *Rho*$^{-/-}$ (**G**) retinas stained with anti-Aif (red) and TUNEL (green) confirming nuclear translocation of Aif in dying cells (arrows). Some TUNEL positive cells do not show nuclear translocation of Aif (arrowhead). Merge: merged images of the red, green and blue channels. Nuclei were stained with DAPI (blue).

Figure S2. Analyses of Calcium in murine mutant Rho photoreceptors. (**A**) Flow cytometry characterization of the cell population dissociated from a PN16 Rho$^{+/-}$ retina. The cell population and the rod photoreceptor cells labeled with the 1D4 anti-Rho antibody (Q2 gate) show a bimodal pattern as previously reported (67). This photoreceptor population was gated for all subsequent studies. (**B**) Histogram representing percentages of cells with high levels of Ca^{2+}. A significant increase was observed in mutant retinas (*** $P \leq 0.001$). (**C-E**) Flow cytometry outcomes of calcium labeling with Fluo-4 AM (fluorescence intensity on the Y axis) in *P23H*^{Tg} and *Rho*$^{+/+}$ at PN10 (**C**); in *Rho*$^{P23H/-}$ and *Rho*$^{+/-}$ at PN16 (**D**) and in *Rho*$^{-/-}$ and *Rho*$^{+/+}$ at PN45 (**E**). Gates applied measure the cell percentages with high level of Ca^{2+}.

Figure S3. Quantification of experiments shown in figure 5. Mice were treated either with salubrinal (SAL, green bars) or calpastatin peptide (CS, blue bars) or with salubrinal and calpastatin peptide together (CS+SAL, black bars). Protein extracts from retinas treated with drugs or treated with vehicle only (mock, white bars) were analyzed at the age

of PN9 for *P23H*^{Tg} and PN16 for *Rho*$^{P23H/-}$. (**A-B**) Quantifications of western blots of total protein extracts show significant increase of phosphorylated Ire1 after treatment with SAL and CS+SAL in *P23H*^{Tg} (**A**) or in *Rho*$^{P23H/-}$ (**B**) retinas. No effect on Ire1 phosphorylation was observed after treatments with CS only. (**C-D**) Quantifications of RT-PCR analyzing the spliced form of *Xbp1* (*sXbp1*) confirm activation of the Ire1 pathway after treatment with SAL and CS+SAL in *P23H*^{Tg} (**C**) or in *Rho*$^{P23H/-}$ (**D**) retinas. No effect on *Xbp1* splicing was observed after treatment with CS only. (**E-F**) Quantifications of immunoblots of total protein extracts show no significant change of phosphorylated Perk in either *P23H*^{Tg} (**E**) or *Rho*$^{P23H/-}$ (**F**) retinas. (**G-H**) Quantifications of immunoblots of total protein extracts show significant increase of phosphorylated Eif2α after treatment with SAL and CS+SAL in *P23H*^{Tg} (**G**) and in *Rho*$^{P23H/-}$ (**H**) retinas. No effect on Eif2α phosphorylation was observed after treatment with CS only. (**I-J**) Quantifications of immunoblots of nuclear protein extracts show significantly reduced nuclear translocation of Aif after treatment with SAL or CS in *P23H*^{Tg} (**I**) and in *Rho*$^{P23H/-}$ (**J**) retinas. (**K-L**) Quantifications of immunoblots of total protein extracts show significant increase of Bip/Grp79 after treatment with SAL and CS+SAL in *P23H*^{Tg} (**K**) and in *Rho*$^{P23H/-}$ (**L**) retinas. No effect on Bip/Grp79 levels was observed after treatment with CS only. *** $P \leq 0.001$; ** $P \leq 0.01$; * $P \leq 0.05$ t-Student comparing treated retinas with the corresponding controls (white bars).

Figure S4. Histological analysis of treated retinas. (**A, C, E**) Histological analysis by Hematoxylin-Eosin staining of *P23H*^{Tg} (**A**), *Rho*$^{P23H/-}$ (**C**) and *Rho*$^{-/-}$ (**E**) mutant retinas after treatments with vehicle only (mock) or with salubrinal (SAL) or calpastatin peptide (CS) or with calpastatin peptide and salubrinal together (CS+SAL). ONL= outer nuclear layer; INL = inner nuclear layer; GCL= ganglion cell layer. Scale bar: 100μm. (**B, D**) Immunofluorescence analysis of RHO protein (green) in *P23H*^{Tg} (**B**) and *Rho*$^{P23H/-}$ (**D**) retinas after treatments with vehicle only (mock) or with salubrinal (SAL) or calpastatin

peptide (CS) or with calpastatin peptide and salubrinal together (CS+SAL). Sections were co-stained with the anti-PERK antibody (red) identifying the ER. Scale bar: 20μm.

Abbreviations

Aif: apoptosis-inducing factor

ER: endoplasmic reticulum

ERAD: ER-associated degradation

RHO: human Rhodopsin

Rho: murine Rhodopsin

RP: retinitis pigmentosa

UPR: unfolded protein response

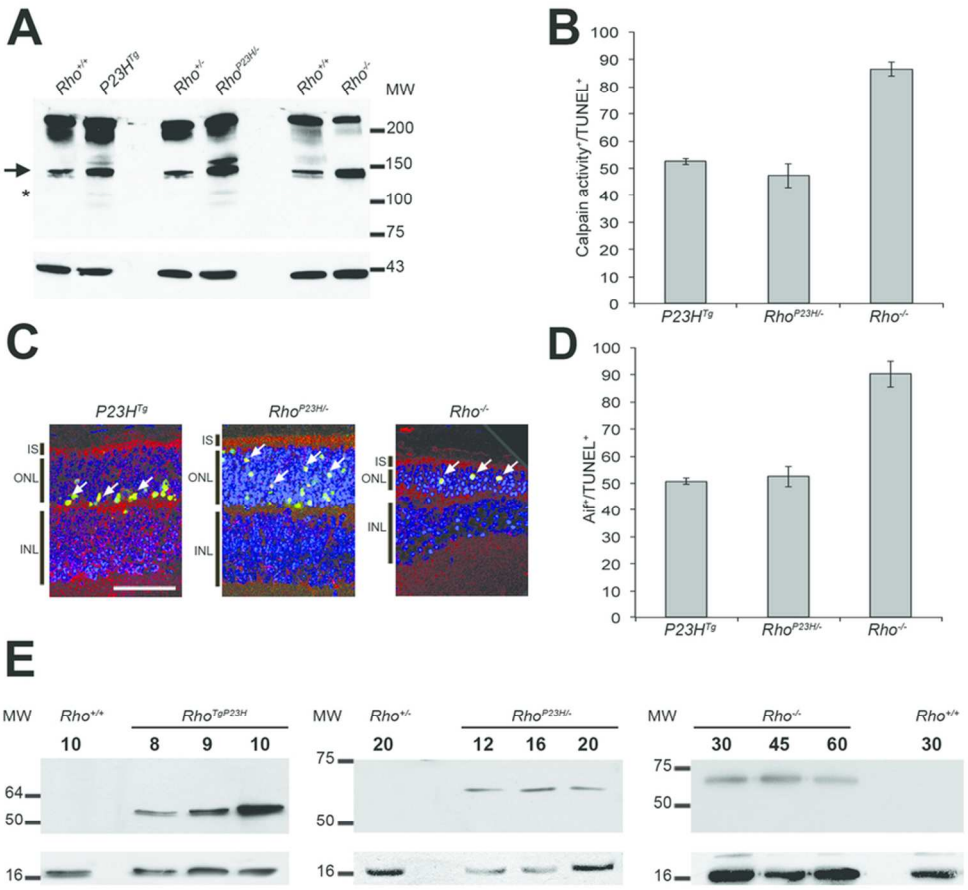

Figure 1
80x75mm (300 x 300 DPI)

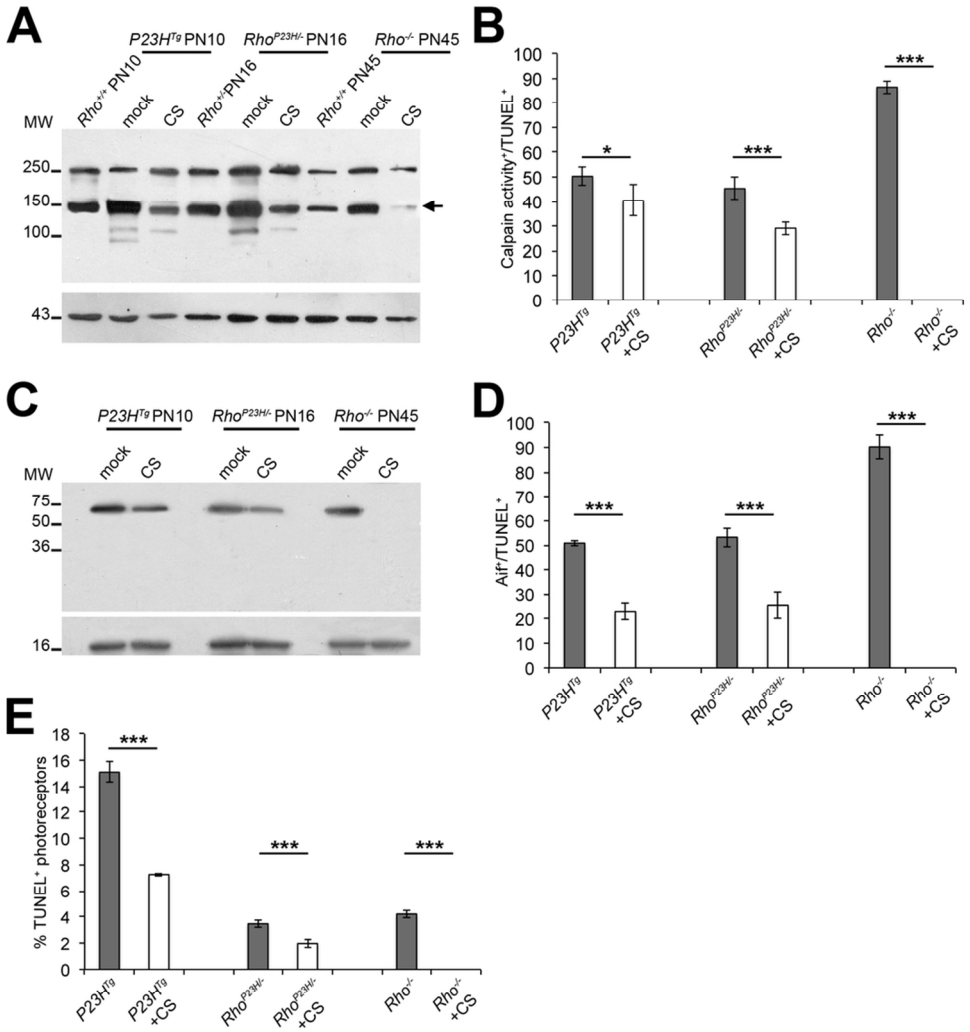

Figure 2
93x101mm (300 x 300 DPI)

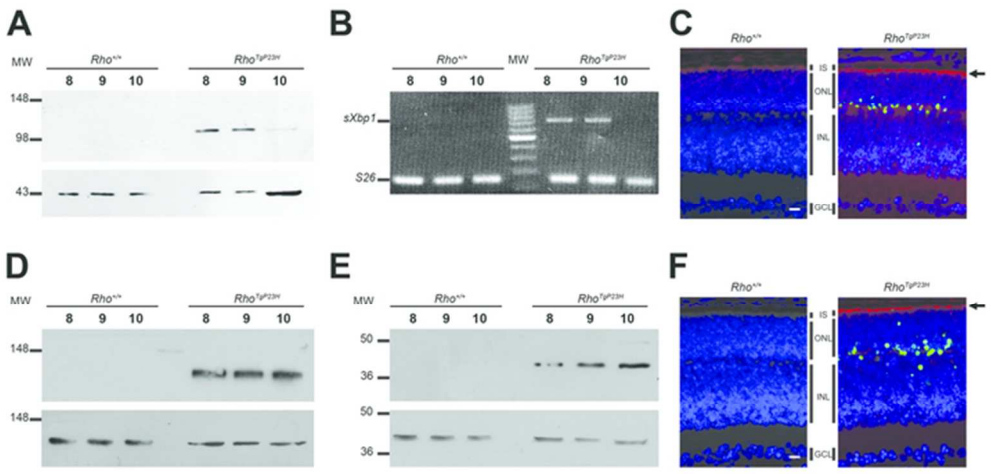

Figure 3
61x30mm (300 x 300 DPI)

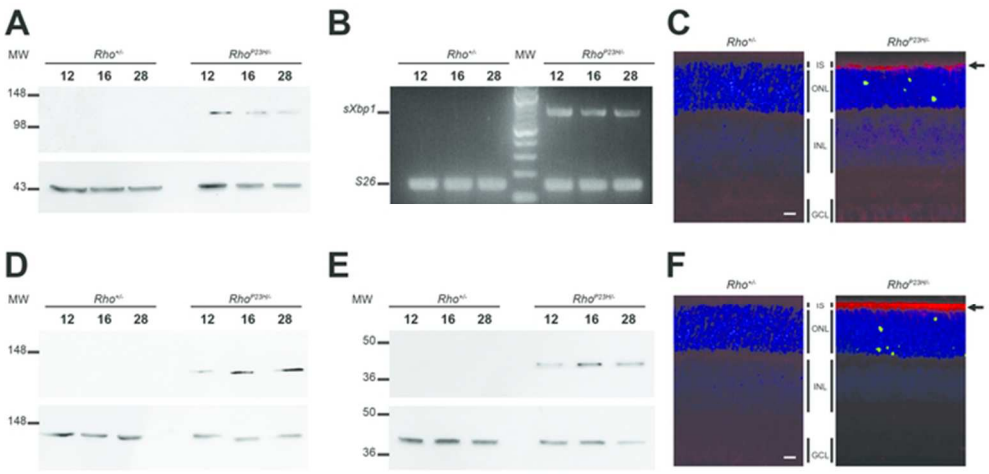

Figure 4
61x30mm (300 x 300 DPI)

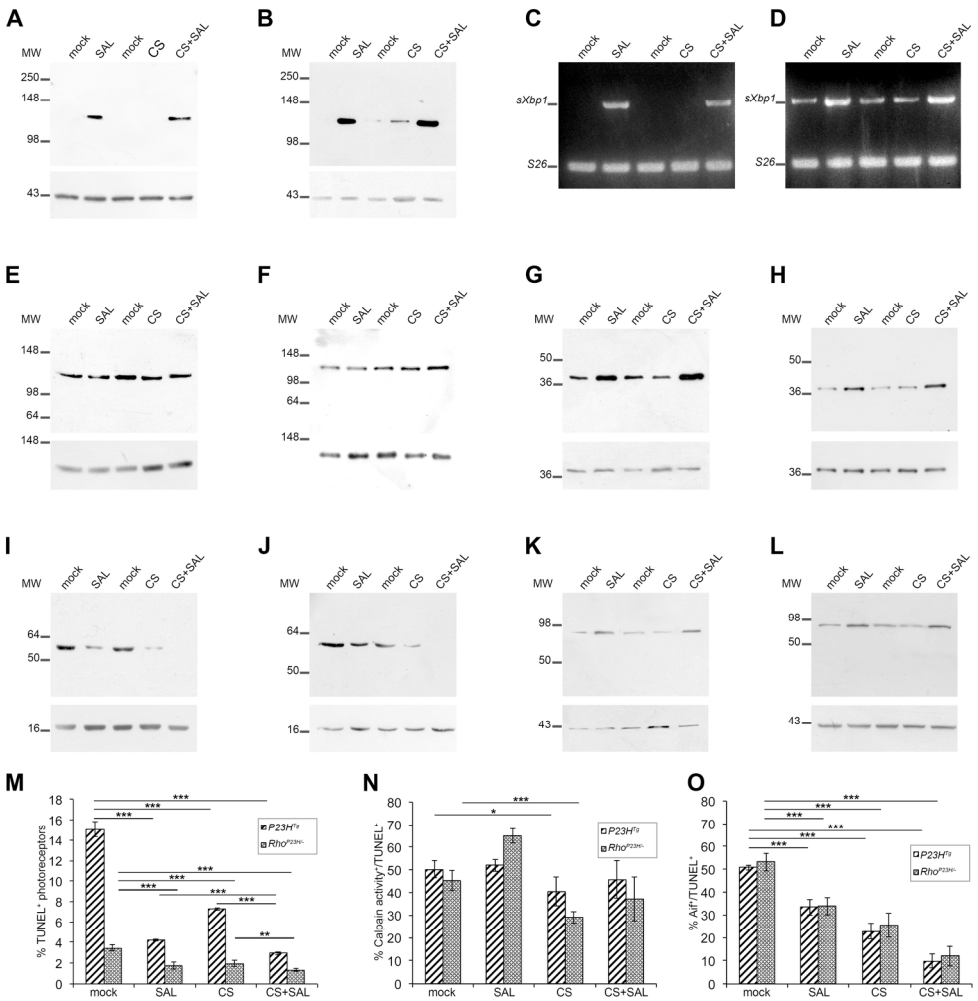

186x192mm (300 x 300 DPI)

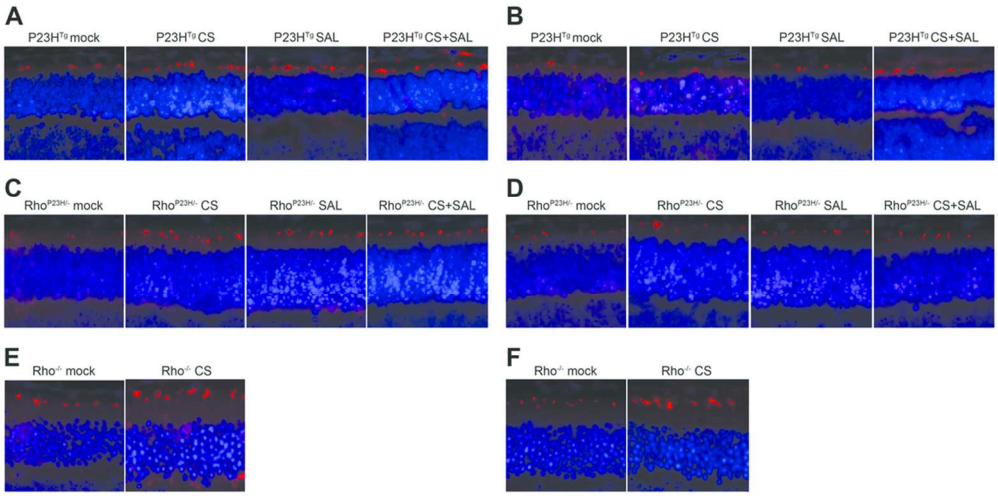

Cone analysis after treatments: Retina sections were analyzed by immunofluorescence with anti-OPN1MW (M cone opsin) (A, C, E) or anti-OPN1SW (S cone opsin) (B, D, F), shown in red, in mock treated P23H^{Tg} (A-B), Rho$^{P23H/-}$ (C-D), Rho$^{-/-}$ (E-F) mice or treated with calpastatin peptide (CS), salubrinal (SAL) or calpastatin peptide and salubrinal (CS+SAL).

98x57mm (300 x 300 DPI)